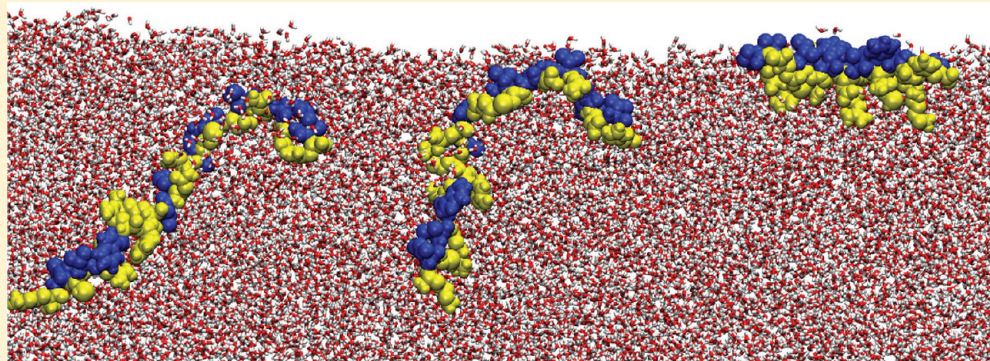


Adsorption, Folding, and Packing of an Amphiphilic Peptide at the Air/Water Interface

Ozge Engin and Mehmet Sayar*

College of Engineering, Koç University, 34450, Istanbul, Turkey

Supporting Information



ABSTRACT: Peptide oligomers play an essential role as model compounds for identifying key motifs in protein structure formation and protein aggregation. Here, we present our results, based on extensive molecular dynamics simulations, on adsorption, folding, and packing within a surface monolayer of an amphiphilic peptide at the air/water interface. Experimental results suggest that these molecules spontaneously form ordered monolayers at the interface, adopting a β -hairpin-like structure within the surface layer. Our results reveal that the β -hairpin structure can be observed both in bulk and at the air/water interface. However, the presence of an interface leads to ideal partitioning of the hydrophobic and hydrophilic residues, and therefore reduces the conformational space for the molecule and increases the stability of the hairpin structure. We obtained the adsorption free energy of a single β -hairpin at the air/water interface, and analyzed the enthalpic and entropic contributions. The adsorption process is favored by two main factors: (1) Free-energy reduction due to desolvation of the hydrophobic side chains of the peptide and release of the water molecules which form a cage around these hydrophobic groups in bulk water. (2) Reduction of the total air/water contact area at the interface upon adsorption of the peptide amphiphile. By performing mutations on the original molecule, we demonstrated the relative role of key design features of the peptide. Finally, by analyzing the potential of mean force among two peptides at the interface, we investigated possible packing mechanisms for these molecules within the surface monolayer.

I. INTRODUCTION

Small peptide molecules with a well-defined β -hairpin secondary structure have gained increased attention over the past decade. These molecules provide ideal models for studying amyloid formation, which triggers diseases such as Alzheimer's,^{1,2} Huntington's,³ and diabetes.^{4,5} Molecular precision and specific control of intermolecular interactions among these molecules bring up the opportunity to design various assemblies such as fibrils,^{6–9} cylindrical micelles,¹⁰ nanotubes,^{10–12} or monolayers.¹³ Furthermore, self-assembly into such nanostructures can be triggered by environmental stimulus such as pH, temperature, or light. Characteristic properties of amino acids, such as responsiveness, chemical and biological modularity, and recognition by living organisms make peptide-based systems indispensable tools for medical purposes. Among the medical application areas some of the most important are tissue engineering,¹⁴ regenerative medicine,¹⁵ gene and drug delivery,^{16,17} biosensors,^{18,19} and hydrogels.^{20–22} A key requirement for many

of these application areas is that these molecules should exhibit a well-defined and stable equilibrium conformation under stringent conditions and self-assemble to enable bottom-up design strategies.^{9,10,23–25}

In addition to the above-mentioned properties, β -hairpins can also be considered as model folding motifs for globular proteins.^{26,27} In this respect, they provide important insights into the protein folding problem and also help improve secondary structure prediction algorithms with a “fragment-based approach”, as already discussed in the study of Ho and Dill.²⁸ Similarity with globular proteins also provides the opportunity to improve peptide design strategies: survey of structures in the Protein Data Bank enables identification of novel sequences for loop and strand residues in β -hairpin structures.²⁹

Received: July 5, 2011

Revised: January 9, 2012

Published: January 23, 2012

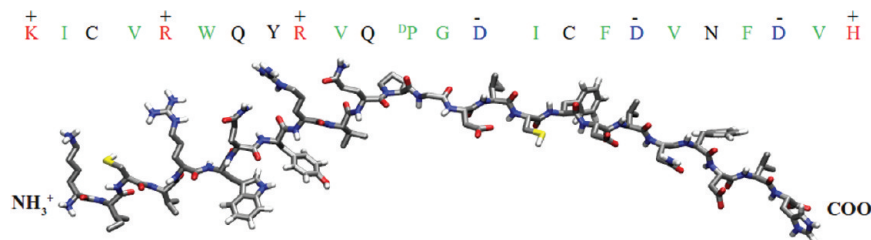


Figure 1. Primary sequence of the peptide under study. Residues are labeled with one-letter coding. Positively and negatively charged residues are shown in red and blue, whereas nonpolar and polar residues are shown in green and black, respectively. ^DPro-Gly residues located in the center lead to a kinked conformation.

Another important feature of these molecules is their ability to fold below microsecond time scales, which makes these systems accessible via molecular dynamics (MD) simulations. In previous computational studies, key determinants of β -hairpins, such as turn,^{30–34} hydrophobic,^{34–40} and polar residues^{34,39,40} as well as their relative weights on the stability of the structure^{41–44} were investigated. Close similarities to amyloid formation have guided most of the earlier computational studies to investigate folding mechanisms and energy landscapes of different β -hairpin structures.^{45–60}

In this study, we analyzed the adsorption, folding, and surface monolayer formation by a 24-residue amphiphilic peptide (Figure 1) designed by the group of Raymond Tu.⁶¹ The molecule exhibits several key design features: The peptide sequence has an alternating array of hydrophobic and hydrophilic residues, which gives the molecule an amphiphilic character. ^DPro-Gly residues in the center of the sequence create a kink and strongly favor formation of a β -hairpin secondary structure. Furthermore, the sequence of the peptide is chosen such that the first half of the molecule carries mostly positively and the second half carries mostly negatively charged residues.

Here, by using MD simulations, we analyzed the simultaneous adsorption and folding of the peptide molecule at the air/water interface and calculated the adsorption free energy. We highlighted the role of key design features required for the formation and stability of the β -hairpin conformation via *in-silico* mutations. Furthermore, by calculating the potential of mean force between two β -hairpin peptides at the interface, we investigated packing of these molecules into surface monolayers.

II. METHODS

MD simulations were performed with the Gromacs 4.0 simulation package.⁶² Temperature was kept constant at 298 K via a Berendsen thermostat with a coupling time of $\tau_T = 0.1$ ps. For constant pressure simulations, a Berendsen barostat⁶³ was used with a coupling time of $\tau_P = 0.5$ ps.

The GROMOS GS3A6 force field,⁶⁴ which is parametrized to reproduce hydration free energies of amino acid analogues, was used for peptides. Water molecules were modeled with SPC/E,⁶⁵ which is known to provide accurate hydration free energies when used together with GROMOS GS3A6.⁶⁶ Bond lengths for water molecules and peptides were constrained via the SETTLE⁶⁷ and P-LINCS⁶⁸ algorithms, respectively.

The particle mesh Ewald method (PME)⁶⁹ was used for electrostatic interactions with a real space cutoff of 1.0 nm and a grid spacing of 0.12 nm. For simulations performed in the presence of an interface, we applied a slab correction for PME.⁷⁰ The correction was applied both to force and potential to produce a pseudo-2D summation, hence breaking the artificial

periodicity along the interface. Lennard-Jones interactions were calculated with a twin-range cutoff scheme of 1.0 and 1.4 nm with the neighbor list updated every 10 steps. A time step of 2 fs was used for the integration. Prior to production MD runs, systems were energy minimized via steepest descent algorithm to remove all possible steric clashes.

The ionization state of each residue was assigned according to pH 7.0, resulting in a total charge of +1 per peptide. Peptide termini were in zwitterionic state in accordance with experimental conditions. One counterion was added for each charged residue of the peptide to maintain neutrality.

The DSSP algorithm⁷¹ implemented in the Gromacs 4.0 package was used for secondary structure analyses. Mutations were done via the WHATIF program.⁷² For hydrogen bonds (H-bonds), analyses angle and distance criteria of 30° and 0.35 nm were used, respectively. Visual Molecular Dynamic program⁷³ was used in the preparation of all molecular graphics.

Simulations of a single peptide in bulk water and in the presence of the air/water interface were performed in the canonical ensemble. In order to create the air/water interface, an equilibrated water box was expanded to three times the height of the original box along the z-direction. The peptide in its kinked conformation (Figure 1) was used as the starting conformation, except in simulations where the turn residues were mutated. The molecule was placed in the middle of the water slab at the beginning of the simulations. Five sets of simulations with different initial conditions are performed for both bulk and interface for the structural characterization of the system.

The adsorption free energy of a single peptide to the air/water interface was calculated via constraint pulling MD simulations. The center-of-mass of the peptide was constrained at 40 different points, with 0.1 nm spacings from the center of the water slab to the upper interface. The position of the interface was defined as the z-coordinate where the density of water drops to half of its bulk value. The average force measured at each constraint distance was integrated by the trapezoidal rule to calculate the potential of mean force (PMF) for peptide adsorption. Standard error estimates were obtained by block averaging,⁷⁴ taking into account possible long time correlations. On average, 40 ns simulations were performed for each constraint point.

In order to calculate the association free energy between a pair of β -hairpin peptides placed at the air/water interface, umbrella sampling^{75,76} was used. The peptides were pulled away over 400 ps until the center-of-mass distance between the two peptides was 4.0 nm. The pulling force was confined to the interface ($x-y$ plane) and a spring constant of 1000 kJ mol⁻¹ nm⁻² and a pull rate of 0.01 nm/ps were used. Snapshots from these trajectories were used to generate starting configurations for the

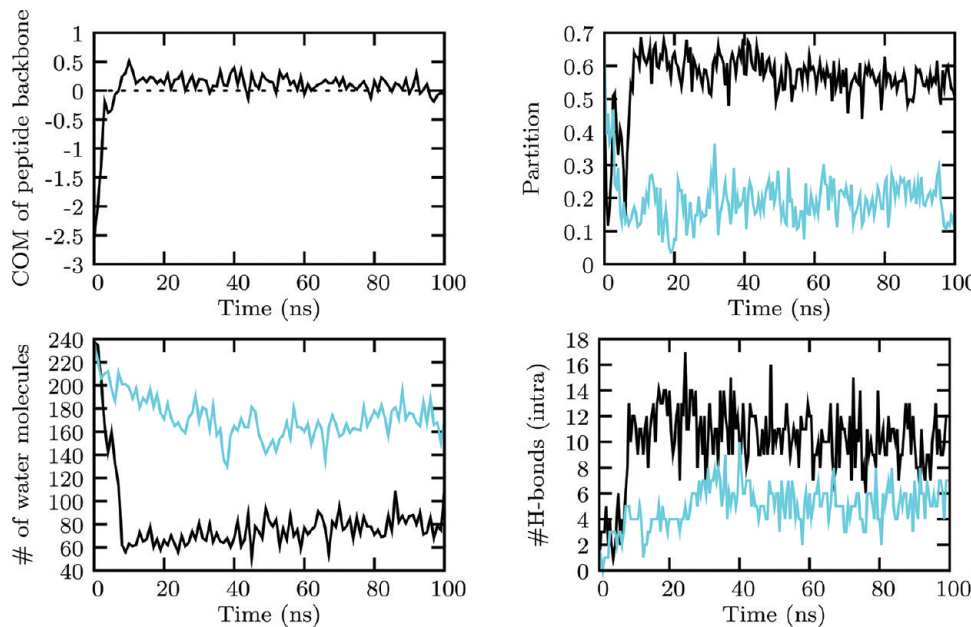


Figure 2. Adsorption of the peptide to the air/water interface and structural changes in the system during a 100 ns MD simulation (solid black line). Results from a bulk water simulation for the same structural quantities are also given for comparison (cyan color). Top left: Distance of the center of mass of the peptide from the upper air/water interface (marked by the zero line). Top right: Segregation of the hydrophobic and hydrophilic residues of the peptide measured as the distance between the center-of-mass of the two groups. Bottom left: Number of water molecules in contact with the hydrophobic residues of the peptide. Bottom right: Number of intrapeptide hydrogen bonds.

umbrella sampling windows. The windows contained configurations with increasing center-of-mass spacings of 0.1 nm increments up to 2.5 nm, and 0.2 nm increments beyond. A total of 32 windows was used and a 10 ns MD simulation was performed for each. Results were analyzed with the weighted histogram analysis method (WHAM).⁷⁷ Error analyses were performed using the bootstrap method.⁷⁸

III. RESULTS AND DISCUSSION

A. Single Peptide Molecule in a Water Slab. The peptide molecule under study is designed with the goal of obtaining an amphiphilic molecule with a β -hairpin structure at the air/water interface. Hence, we begin our analysis by looking at the conformational behavior of a single peptide molecule in a water slab by performing MD simulations under constant volume and temperature. A water layer of 5 nm thick was centered in a box of height 15 nm so that two interfaces were present in the system. The remaining part of the box was left as a vacuum. The peptide molecule was placed in the center of the water slab in a kinked conformation (Figure 1). In order to understand the influence of the interface, we will compare the interface simulation with a bulk water simulation which was performed under identical conditions.

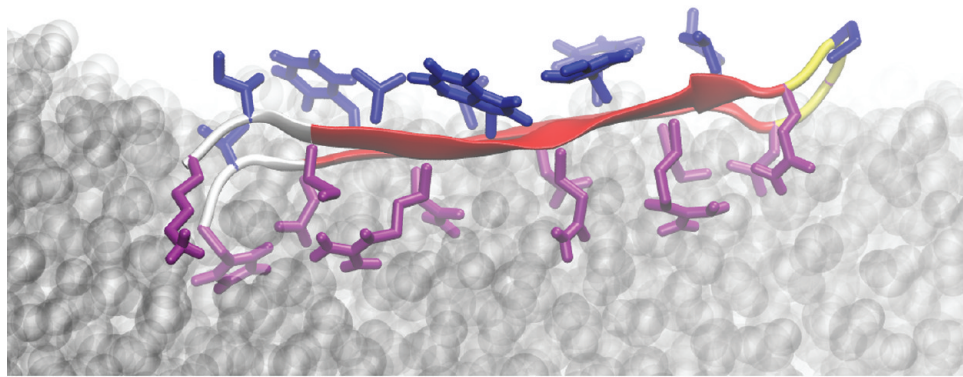
As soon as one or more of the hydrophobic residues of the peptide got in close proximity of the interface, the rest of the molecule was also pulled, leading to the adsorption of the whole peptide molecule. Time-line data for the distance of the center-of-mass of the peptide from the upper air/water interface shows that (Figure 2, top left) in this particular simulation the adsorption took place after ~ 8 ns. The trajectory for the adsorption and folding of the peptide is available as Supporting Information S1. Once the molecule was adsorbed, it remained at the interface for the remainder of the simulation. A representative snapshot of the peptide after it was fully equilibrated at the interface is shown in Figure 3a, where the interface is shown

from the side, the top part being the vacuum (air) and the bottom part being the water layer (gray bubbles). Also shown in Figure 3b is a representative conformation of the same peptide in bulk water. As opposed to the well partitioned and ordered structure of the peptide at the interface, in bulk water, the molecule is frustrated between formation of a secondary structure and shielding of the hydrophobic side chains from water.

Both at the interface and in bulk, the peptide adopted a β -hairpin structure, as quantified by the DSSP analysis (Figure 4). At the interface, adoption of the β -hairpin secondary structure and adsorption took place simultaneously, as marked by the appearance of the red bands in the DSSP plot around ~ 8 ns (Figure 4a). The fraction of the molecule in β -sheet conformation fluctuated over time; however, these fluctuations remained as small, local perturbations on the backbone dihedral angles, so that the two arms of the β -hairpin remain aligned for the course of the simulation (see Supporting Information S2). The presence of the interface forced the β -hairpin to remain flat, whereas in bulk the structure was slightly twisted (Figure 3).

The flattened secondary structure at the interface is driven by the complete partitioning of the hydrophobic and hydrophilic side chains. Time-line data for the distance between the center-of-mass of the hydrophobic and hydrophilic side chains in Figure 2 (top right) and also the representative snapshots in Figure 3 show that, as opposed to the interface, in bulk water this partitioning cannot be completed. In bulk, even though the hydrophobic side chains are driven toward each other via hydrophobic forces, at a single molecule level, complete shielding of hydrophobic side chains from water is not possible. Figure 2 (bottom left) shows the number of water molecules within 0.5 nm of the hydrophobic side chains of the peptide. At the interface, once again, simultaneous with the adsorption, a drastic reduction in number of water molecules in contact with hydrophobic side chains is observed. On the other hand, for bulk, even though a small reduction is seen, in equilibrium,

a)



b)

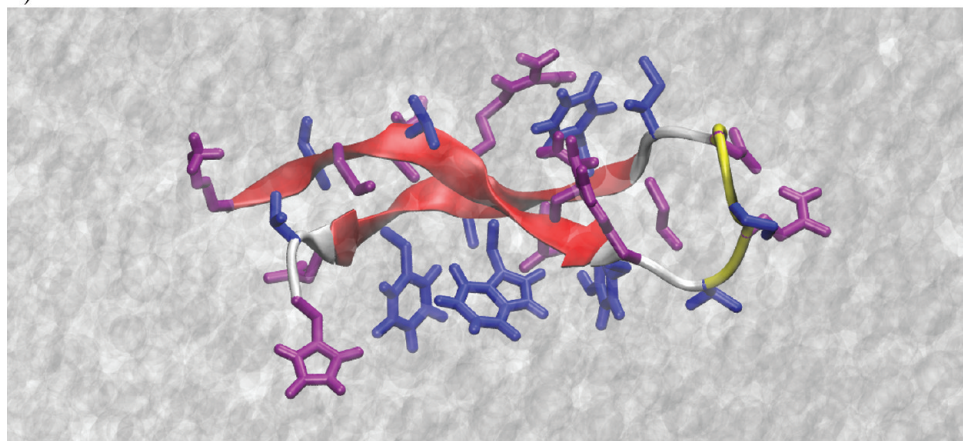


Figure 3. Representative snapshots for the peptide at the air/water interface (a) and in bulk water (b). Hydrophobic and hydrophilic side chains are shown in licorice representation in blue and purple color, respectively. Peptide backbones are colored according to the secondary structure of the molecule as in DSSP analysis (see Figure 4). Transparent gray bubbles correspond to the water molecules.

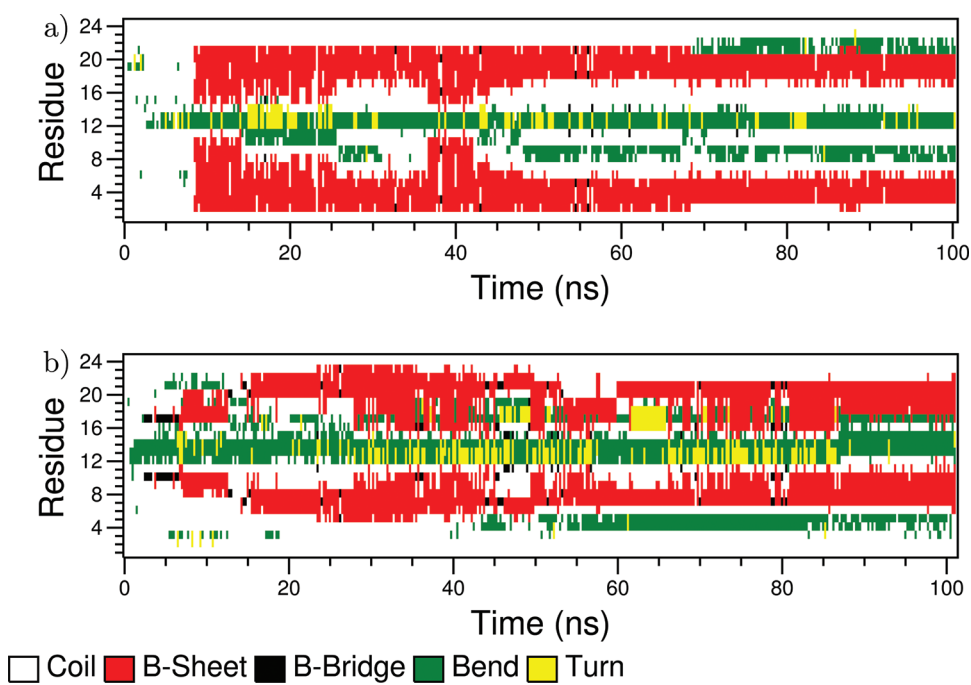


Figure 4. Time evolution of the secondary structure of the peptide in the presence of the air/water interface (a) and in bulk water (b) via DSSP analysis.

a large number of water molecules still remain close to the hydrophobic side chains. The twist in β -hairpin structure is most likely related to the reduction of the water contact area of the hydrophobic side chains. Comparison of the number of intrapeptide H-bonds (Figure 2, bottom right) also reveals that complete partitioning of the hydrophobic/hydrophilic side chains at the interface led to a more stable/ordered β -hairpin structure compared to bulk.

The results presented above are based on plain MD simulations of the peptide in the presence of the interface and in bulk water. In order to test the validity of these observations, we have performed five sets of simulations for both interface and bulk systems. Representative snapshots from these additional simulations are given in Supporting Information S3. Overall, even though these runs differed vastly in terms of the time required for folding and adsorption of the peptide, the final conformation and structural properties were identical to the results presented above.

As noted earlier, after adsorption, the peptide remained at the interface during the course of the 100 ns simulation. This already suggests that the adsorption free energy is much larger than the thermal energy. In order to quantify the free energy of adsorption at the interface, we performed constraint pulling MD simulations. The starting conformation at each constraint point was chosen as a β -hairpin; otherwise, the calculated free energy would have included energetic terms related to peptide folding as well. We did not put any constraints on the peptide to maintain the β -hairpin conformation during simulations. H-bonds formed between the strands were stable enough that, once the peptide adopted the β -hairpin conformation, it did not unfold again at 298 K within the time scale of simulations. In fact, the β -hairpin conformation remained stable up to 500 K in additional runs we performed (results not shown).

The potential of mean force (PMF) during adsorption is shown in Figure 5. PMF is measured as a function of the

to the interface. As the molecule was dragged further above the interface into the air, a sharp increase in the PMF was observed, since hydrophilic side chains strongly oppose this desolvation. Furthermore, pulling of the hydrophilic groups out of water leads to a dramatic disruption of the interface, with several water molecules bridging the gap between the peptide and bulk water. If the molecule is pulled completely into the vacuum, one would expect a flat PMF profile. However, we did not drag the molecule so far out into the vacuum.

Also shown in Figure 5 is the change in the internal energy of the system (cyan colored line). The oscillations are mostly due to higher error bars for the internal energy, which are also shown in the same figure. However, the discrete nature of the hydrophobic side chains along the backbone also plays a role (see Supporting Information S4) especially after part of the molecule gets in contact with the interface (beyond -1.5 nm of the interface). Due to the rigid nature of the hairpin conformation, the peptide molecule tries to maximize its hydrophobic side chain contact with the vacuum under the given constraint distance. Hence, a fluctuating internal energy profile is observed. Interestingly, the internal energy more or less fluctuates around zero for distances as close as 0.1 nm to the interface, despite a large reduction in PMF beyond -1.5 nm, when the molecule touches the interface for the first time. Hence, we conclude that reduction in PMF upon contact with the interface should be mainly due to the entropy gain in the system. This entropy gain is associated with the release of the water molecules which form a cage around the hydrophobic side chains in bulk water. A sharp reduction in the internal energy is only seen when the molecule's hydrophobic/philic parts are completely partitioned right at the interface. This enthalpic contribution should be due to the desolvation of the hydrophobic side chains and increased hydrogen bonding capacity of the water molecules released from the interface upon peptide adsorption.

Free energy of adsorption, ΔG^I , is obtained via eq 1 by integrating the PMF in Figure 5 starting from 1.5 nm below the interface. This position corresponds to the point where the PMF starts to decrease from its bulk value. Defining a free energy for partitioning between the bulk and the interface is not straightforward, since it depends on the amount of bulk that is present below the interface, as we discussed in our previous study.⁷⁹ We determine the free energy with respect to a reference thickness of the bulk layer l :

$$\Delta G^I = -k_B T \log \left[\frac{1}{l} \int_{\text{well}} \exp \left(-\frac{W(z)}{k_B T} \right) dz \right] \quad (1)$$

where $W(z)$ is the PMF with a reference value of $W(0) = 0$ in the bulk. The integration is performed over the PMF well. The precise boundaries of the well are not critical, because of the exponential weighting. This calculation yields $\Delta G^{1.5\text{nm}} = -50.29 \pm 2.94$ kJ/mol, showing that the adsorption of the amphiphilic peptide at the air/water interface is highly favorable.

In our earlier study,⁷⁹ we showed that the adsorption free energy of small amphiphilic peptides follows a linear trend proportional to the number of hydrophobic groups present in the molecule. Within the linear regime, adsorption free energy is reduced by ~ 10 kJ/mol for each hydrophobic group present. The amphiphilic β -hairpin peptide contains around 11 hydrophobic groups, and if the adsorption free energy remained within the linear regime, this would yield ~ -110 kJ/mol. Notably, the value obtained from the PMF calculation in this

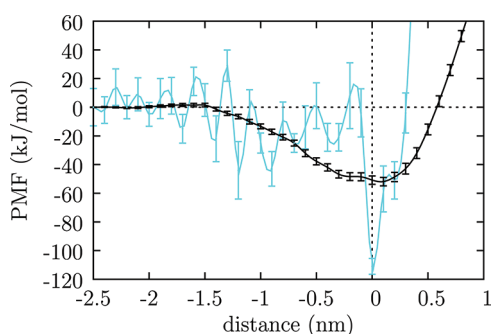


Figure 5. PMF for adsorption of a single peptide molecule to the air/water interface as a function of the distance from the upper air/water interface (solid black line with the error bars). The enthalpic contribution, measured as the change in the average potential energy of the system, is also shown with a cyan colored line together with the associated error bars.

distance of the peptide center-of-mass from the upper air/water interface. The flat region of the PMF corresponds to bulk water, where there is no preference for the orientation of hydrophobic/philic groups of the peptide. Beginning from -1.5 nm, the hydrophobic side chains of the peptide started touching the air/water interface; hence, the molecule was drawn toward that direction. At the PMF minimum, the partitioning of the hydrophobic and hydrophilic side chains was optimized with respect

study is less than half of this linear estimate. This large difference is a direct result of the amphiphilic β -hairpin peptide's ability to adopt a secondary structure in bulk unlike the small amphiphilic peptides in our earlier study. Secondary structure adoption in bulk enables partial shielding of the hydrophobic residues even in bulk water, and therefore, the measured adsorption free energy is significantly reduced compared to the linear regime.

B. Conformational Stability against Mutations. We analyzed the role of the alternating hydrophobic/hydrophilic residue pattern and turn residues on both the adsorption process and the formation/stability of the β -hairpin structure via *in silico* mutation experiments.

In order to investigate the influence of the alternating hydrophobic/hydrophilic residue pattern of the original molecule, we mutated all the hydrophobic residues to glycine. This led to two drastic changes in the behavior of the peptide. First, as seen from the time line evolution of the center-of-mass of the peptide molecule (Figure 6b), the absence of the hydrophobic

nature due to this mutation, this is an expected result. More surprisingly, the molecule also cannot adopt the β -hairpin conformation as seen in the representative snapshot (Figure 6a) and evidenced by the DSSP data (Figure 6c). Hence, we conclude that the presence of the turn region alone is not sufficient to trigger formation of a β -hairpin structure, and the hydrophobic driving force in water is essential for secondary structure formation.

The presence of the turn residues, D Pro-Gly, is another key feature of the peptide's design. Mutation of these residues to alanine disrupts the kinked geometry of the peptide. Since the molecule still maintains its amphiphilic nature, the peptide adsorbs to the air/water interface, as shown in the representative conformation of the peptide at the interface (Figure 7a)

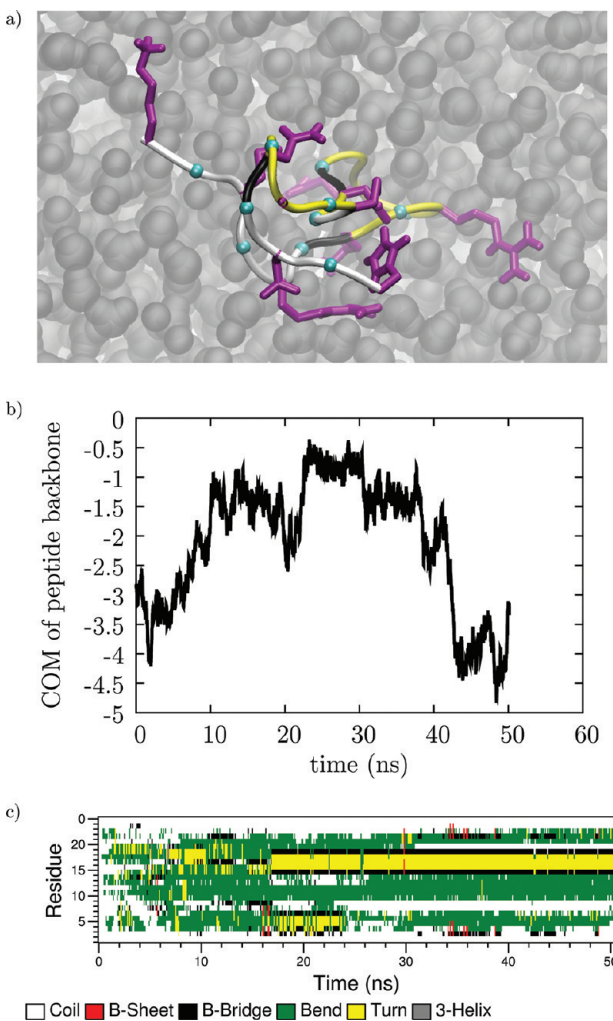


Figure 6. A representative conformation of the peptide with all hydrophobic residues mutated to glycine (a). This mutation prevents both adsorption to the interface and formation of a stable beta-hairpin structure, as evidenced by the center-of-mass motion of the peptide (b) and DSSP data (c), respectively.

residues prevents adsorption of the peptide to the air/water interface. Considering that the peptide has lost its amphiphilic

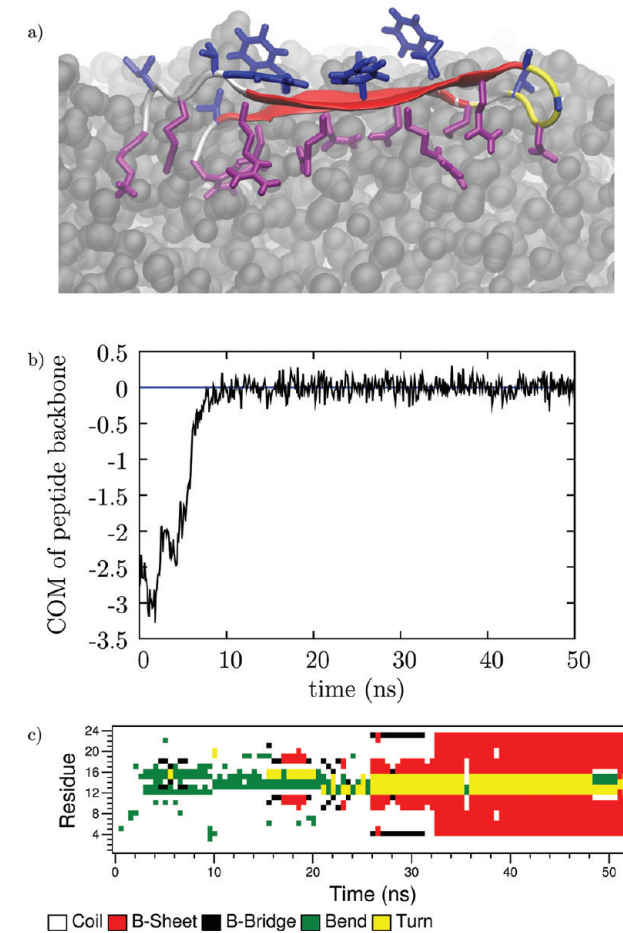


Figure 7. Mutation of the turn residues D Pro-Gly with two alanines leads to the loss of the perfect registry among the β -strands of the hairpin. The peptide still adsorbs to the interface as seen in the representative conformation (a) and the time evolution of the distance of the center of mass of the peptide from the upper air/water interface (b). DSSP data shows the formation of the β -hairpin and slightly off centered strand regions (c).

and time-line data for the center-of-mass motion of the peptide (Figure 7b). The absence of the turn region also does not hinder the formation of the β -hairpin structure, as evidenced by the DSSP data (Figure 7c). However, the perfect registry of the arms of the β -hairpin structure is lost, and the peptide is bent at an arbitrary position. Note that, unlike the original molecule, in this case, adsorption and folding are not simultaneous.

More than 20 ns after adsorption, the peptide finally adopts the β -hairpin structure.

C. Molecular Packing at the Interface. The magnitude of the adsorption free energy for the peptide molecule suggests that these molecules can form a monolayer film at the interface and thereby reduce the surface tension significantly. β -hairpin secondary structure and confinement to the interface significantly reduce the conformational flexibility of the individual molecules. Even in this fairly restricted conformational space, predicting the packing of peptide molecules within a surface monolayer is quite challenging. Strong adsorption free energy rules out conformations where the hydrophobic side of the β -hairpin faces toward water. In trial runs, we observed that starting from such a flipped conformation leads to an immediate back flipping of the molecule so that hydrophobic/philic partitioning with respect to the interface is restored (see Supporting Information S5). If one assumes that the neighboring molecules should be aligned with respect to each other, maximizing the interpeptide hydrogen bonds, parallel and antiparallel orientations (Figure 8) remain as possible targets.

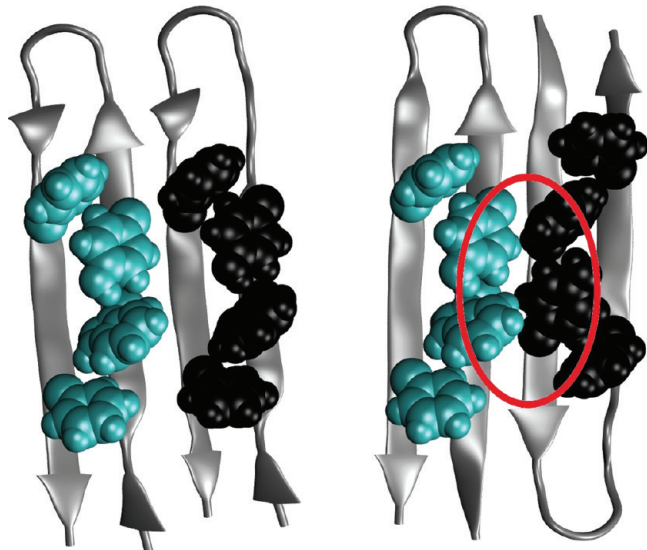


Figure 8. Parallel and antiparallel packing of molecules at the interface (looking down from the air side). Aromatic side chains of the peptides are shown with their van der Waals radii.

In order to compare parallel and antiparallel orientations, we calculated the PMF among two β -hairpin peptides at the air/water interface. In these calculations, a pair of peptide molecules is placed at the air/water interface and the mean constraint force is calculated for a set of center-to-center spacings among them. The surface area for the interface is chosen large enough to ensure that PMF calculation is not biased by the influence of the periodic images. The constraint distance is increased until the peptides are completely isolated from each other, and the PMF curve is obtained by integrating over the constraint distance.

As seen in Figure 9, the parallel and antiparallel orientations lead to optimum spacings (PMF minimum) of 0.98 and 1.05 nm, respectively. Despite the larger spacing, the antiparallel orientation is energetically more favorable compared to the parallel one, with an association free energy of 103.70 ± 0.05 kJ/mol for antiparallel and 93.76 ± 0.02 kJ/mol for parallel orientation. The larger spacing of the antiparallel orientation is a result of the charge–charge interactions and packing

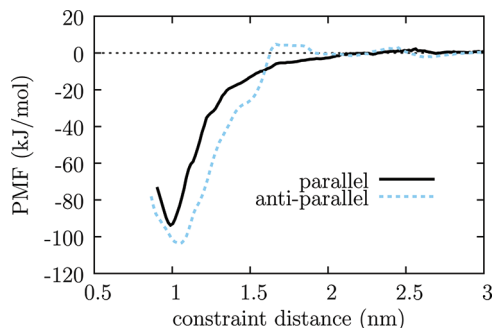


Figure 9. PMFs obtained from umbrella sampling simulations of parallel and antiparallel packed molecules at the air/water interface. The errors associated with energy minima are 0.05 and 0.02 kJ/mol for antiparallel and parallel orientations, respectively.

of the aromatic side chains. Due to the design of the peptide molecule, the N-terminus arm is positively and the C-terminus arm is negatively charged. Parallel orientation places the peptides such that a negative arm is adjacent to the positive arm of the neighboring peptide. In the antiparallel orientation; however, the like-charged arms are placed adjacent to each other. Hence, in order to reduce the repulsion, the center-to-center optimum spacing between the molecules remains slightly larger for the antiparallel orientation. However, even for the antiparallel orientation, the closeness of these charged groups is not much of a problem for the peptides, since high dielectric constant of water and 1 nm center-to-center spacing among peptides lead to decreased repulsion.

As highlighted in Figure 8, the antiparallel orientation leads to close contacts among aromatic side chains in the vacuum phase, which partially accounts for the lower association free energy of antiparallel orientation. Also note that the association free energy is not only a function of the peptides, but also surface tension plays a role in determining its magnitude. The antiparallel orientation leads to a slightly higher surface coverage ($10\text{--}12\text{ nm}^2/\text{dimer}$) and therefore shields more water molecules from the interface. Hence, this increased shielding effect also contributes to the lower association energy among the peptides in the antiparallel orientation.

One might argue that the optimum spacing among peptides might be influenced by the presence of other peptides surrounding them. In order to test this, we performed simulations with four peptides at the air/water interface for both parallel and antiparallel orientations, and monitored the spacing between the two central peptides among the four. The average spacing obtained is identical to the results from the pair of peptide molecules; hence, we conclude that the intermolecule spacing is not significantly influenced by the presence of neighboring peptides.

Note that the PMF curves also provide a justification for the initial assumption that the neighboring peptide molecules should be aligned with respect to each other. During the calculation, the peptide molecules are simulated at increasing constraint distances for the center-to-center separation. The PMF minimum is observed when the peptides are perfectly aligned with respect to each other.

In order to test the optimum packing distances obtained from PMF curves, we also performed simulations of a slab of water where the interfaces are covered with 32 peptides each. Since finding the global energy minimum of such a large system starting from a random conformation is not possible, here we only aim to test the stability of a monolayer build according to the PMF results discussed above. The molecules are initially aligned with respect to each other into stripes, so that we have

eight molecules in each one of the four stripes. In order to allow fluctuations in box size, the simulations are performed with anisotropic pressure coupling. Starting from the antiparallel system, we performed simulations of the system under different lateral pressure values. Note that, due to the anisotropic nature of these films, pressure (and spacing) along the stripes of peptides and perpendicular to them should be independent from each other. However, for simplicity we applied the same pressure in both directions.

At a lateral pressure of $p_{xx} = p_{yy} = -60$ bar, which corresponds to a surface tension of 36.3 dyn/cm, the antiparallel packed surface film displayed a center-to-center spacing of 1.05 nm for the molecules, consistent with the PMF result. The average stripe thickness was obtained as 3.67 nm from this simulation. Next, we applied the same lateral pressure (-60 bar) to the parallel system and this gave us a center-to-center spacing of 1.00 nm and stripe thickness of 3.55 nm. Hence, we conclude that, in agreement with the PMF analysis, the antiparallel packing is less dense compared to the parallel one. In Figure 10,

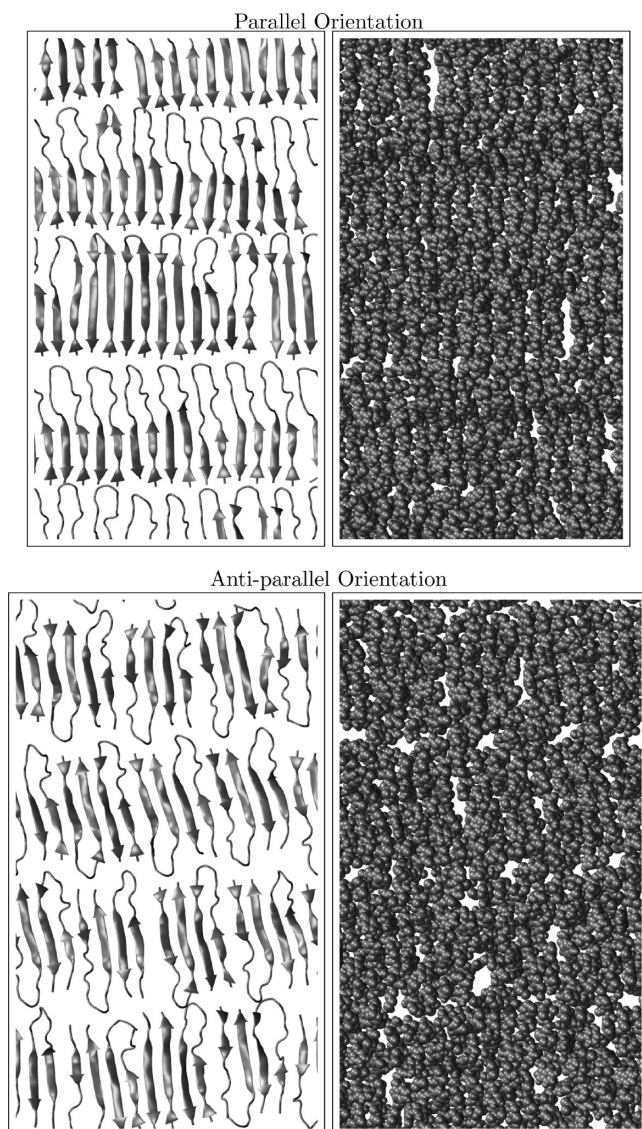


Figure 10. Monolayer of peptides in parallel (top) and antiparallel (bottom) orientation at the air/water interface, where both systems are equilibrated with a lateral pressure of -60 bar. Only the molecules at the top layer of the water slabs are shown from the air side of the interface.

equilibrium snapshots from these systems are shown for parallel (top) and antiparallel (bottom) orientation. The box sizes are shown to scale with the actual equilibrium dimensions. Only the upper interface is shown looking down from the air side of the interface. The cartoon representation shows that, in both cases, individual peptides preserve the β -hairpin structure. In general, the parallel orientation displays a much more ordered monolayer. Small patches of water are exposed to vacuum for both orientations, as seen in the space-filling representations (on the right). Note that antiparallel configuration creates slightly larger exposure of water to vacuum. For the lateral pressure of -60 bar, the partitioning of the hydrophobic/hydrophilic side chains was mostly preserved with only a few side chains flipping to the unfavorable (hydrophobic/hydrophilic) side of the interface.

IV. CONCLUSIONS

In this study, we analyzed adsorption, folding, and packing into a surface monolayer of an amphiphilic peptide in the presence of the air/water interface. MD simulations of a single peptide molecule in a water slab show that adsorption to the interface and adoption of the β -hairpin secondary structure take place simultaneously. Our earlier results⁸⁰ on the conformational preference of these molecules in bulk water suggested that these molecules adopt a β -hairpin structure even in the absence of an interface. However, in this study, we have shown that the presence of the interface leads to ideal partitioning of the hydrophobic and hydrophilic side chains of the molecule and thereby stabilizes it, by eliminating alternative conformations observed in bulk water.

Analysis of the adsorption free energy for these molecules suggests that the stiffness of the molecule determines the decomposition of the free energy into enthalpic and entropic terms. The molecule had a fairly rigid structure in the adopted β -hairpin conformation, due to the perfect alignment of the two halves of the molecule and continuous network of hydrogen bonds in between. This rigid nature and the alternating hydrophobic/hydrophilic residue sequence lead to a fluctuating internal energy and a SAS change (see Supporting Information S4) during adsorption to the interface.

We also determined key design features required for adsorption and formation of the β -hairpin conformation. *In-silico* mutations showed that turn residues are essential for perfect registry of the arms of the β -hairpin, whereas hydrophobic residues are required both for adsorption and formation of the β -hairpin structure at the air/water interface and in bulk.

Next, we analyzed the possible arrangement of these peptides within a surface monolayer. The molecules lie flat at the interface to accomplish an optimal partitioning of the hydrophilic/phobic residues. Potential of mean force calculations among two peptide molecules at the interface suggest that these molecules prefer to be aligned with respect to each other, in order to maximize the interpeptide hydrogen bonds. Comparison of the parallel and antiparallel orientations reveals a slightly larger spacing among the molecules for the antiparallel orientation. Hence, in the antiparallel orientation, more water molecules would be shielded from the interface. The antiparallel orientation also displays a lower association free energy compared to the parallel one, due to the closer contact among aromatic residues of neighboring peptides. At a lateral pressure of -60 bar, they display optimum interpeptide spacings that match with our results obtained from umbrella sampling simulations. This corresponds to a surface tension of \approx 36.3 dyn/cm, suggesting that monolayer films of this β -hairpin structure can serve as

surfactants. These analyses based on a pair of peptide molecules at the interface and monolayer simulations give us insight regarding the actual packing of these molecules into continuous surface films. In order to determine the actual reduction in surface tension, further experimental input is necessary, which we hope to accomplish in a future study.

This study gives insights into thermodynamics of adsorption as well as surface tension reduction obtained by monolayers of these β -hairpins. In addition, it also elucidates key determinants required for adsorption, formation, and stability of a β -hairpin peptide. Results obtained from this study should guide future studies regarding the design of novel, functional peptide-based nanomaterials, and help improve peptide-design strategies. Here, the air/water interface may also be used to mimic the hydrophobic/hydrophilic interface of cellular membranes, which simplifies the study of protein-based systems that are surface active and/or self-assemble within membranes.

■ ASSOCIATED CONTENT

Supporting Information

Supporting Information is available for the following: (1) Trajectory for the adsorption and folding of the peptide. (2) The angle between the arms of the β -hairpin structure at the interface. (3) Representative conformations from test runs for verification of the bulk and interface simulation results given above. (4) SAS data for the hydrophobic side chains of the peptide as it approaches the interface. (5) Reorientation of the peptide when hydrophobic and hydrophilic faces of the β -hairpin are facing water and vacuum, respectively. This material is available free of charge via the Internet at <http://pubs.acs.org>.

■ AUTHOR INFORMATION

Corresponding Author

*E-mail: msayar@ku.edu.tr. Phone: +90 212 338 1840.

■ ACKNOWLEDGMENTS

We are thankful to Raymond Tu and his group for sharing their experimental data and inspiring this study. We are also thankful to Berk Hess and Alessandra Villa for scientific discussions. We would like to thank Max Planck Society for financial support through the Partner Group Agreement with Prof. Kurt Kremer's Theory Group at MPIP.

■ REFERENCES

- (1) Cerf, E.; Sarroukh, R.; Tamamizu-Kato, S.; Breydo, L.; Derclaye, S.; Dufrene, Y. F.; Narayanaswami, V.; Goormaghtigh, E.; Ryusschaert, J.; Raussens, V. *Biochem. J.* **2009**, *421*, 415–423.
- (2) Hoyer, W.; Gronwall, C.; Jonsson, A.; Stahl, S.; Hard, T. *Proc. Natl. Acad. Sci. U.S.A.* **2008**, *105*, 5099–104.
- (3) Zuccato, C.; Cattaneo, E. *Prog. Neurobiol.* **2007**, *81*, 294–330.
- (4) Brien, T. D.; Butler, P. C.; Westermark, P.; Johnson, K. H. *Vet. Pathol.* **1993**, *30*, 317–332.
- (5) Dupuis, N. F.; Wu, C.; Shea, J.-E.; Bowers, M. T. *J. Am. Chem. Soc.* **2009**, *131*, 18283–92.
- (6) Pandya, M. J.; Spooner, G. M.; Sunde, M.; Thorpe, J. R.; Rodger, A.; Woolfson, D. N. *Biochemistry* **2000**, *39*, 8728–8734.
- (7) Potekhin, S. A.; Melnik, T. N.; Popov, V.; Lanina, N. F.; Vazina, A. A.; Rigler, P.; Verdini, A. S.; Corradin, G.; Kajav, A. *Chem. Biol.* **2001**, *8*, 1025–1032.
- (8) Zimenkov, Y.; Conticello, V. P.; Guo, L.; Thiagarajan, P. *Tetrahedron* **2004**, *60*, 7237–7246.
- (9) Fairman, R.; Akerfeldt, K. S. *Curr. Opin. Struct. Biol.* **2005**, *15*, 453–463.
- (10) Hartgerink, J. D.; Beniash, E.; Stupp, S. I. *Science* **2001**, *294*, 1684–1688.
- (11) Hartgerink, J. D.; Beniash, E.; Stupp, S. I. *Proc. Natl. Acad. Sci. U.S.A.* **2002**, *99*, 5133–5138.
- (12) Hartgerink, J. D.; Granja, J. R.; Milligan, R. A.; Ghadiri, M. R. *J. Am. Chem. Soc.* **1996**, *118*, 43–50.
- (13) Xu, G.; Wang, W.; Groves, J. T.; Hecht, M. H. *Proc. Natl. Acad. Sci. U.S.A.* **2001**, *98*, 3652.
- (14) Holmes, T. C. *Trends Biotechnol.* **2002**, *20*, 16–21.
- (15) Webber, M. J.; Kessler, J. A.; Stupp, S. I. *J. Intern. Med.* **2010**, *267*, 71–88.
- (16) Branco, M. C.; Schneider, J. P. *Acta Biomater.* **2009**, *5*, 817–831.
- (17) Chow, L. W.; Wang, L.; Kaufman, D. B.; Stupp, S. I. *Biomaterials* **2010**, *31*, 6154–6161.
- (18) Rughani, R.; Schneider, J. P. *MRS Bull.* **2008**, *33*, 530–535.
- (19) Coooper, W. J.; Waters, M. *Curr. Opin. Chem. Biol.* **2005**, *9*, 627–631.
- (20) Branco, M. C.; J., P. D.; Wagner, N. J.; Schneider, J. P. *Biomaterials* **2009**, *30*, 1339–1347.
- (21) Lu, S.; Chen, P. *Front. Mater. Sci. China* **2010**, *4*, 145–151.
- (22) Salick, D. A.; Kretsinger, J. K.; Pochan, D. J.; Schneider, J. P. *J. Am. Chem. Soc.* **2007**, *129*, 14793–14799.
- (23) Aggeli, A.; Bell, M.; Carrick, L. M.; Fishwick, C. W.; Harding, R.; Mawer, P. J.; Radford, S. E.; Strong, A. E.; Boden, N. *J. Am. Chem. Soc.* **2003**, *125*, 9619–9628.
- (24) Burns, D. C.; Flint, D. G.; Kumita, J. R.; Feldman, H. J.; Serrano, L.; Zhang, Z.; Smart, O. S.; Woolley, G. A. *Biochemistry* **2004**, *43*, 15329–15338.
- (25) Dunetz, J. R.; Sandstrom, C.; Young, E. R.; Baker, P.; Van Name, S. A.; Cathopoulos, T.; Fairman, R.; de Paula, J. C.; Akerfeldt, K. *Org. Lett.* **2005**, *7*, 2559–2561.
- (26) Imperiali, B.; Fisher, S. L.; Moats, R. A.; Prim, T. J. *J. Am. Chem. Soc.* **1992**, *114*, 3182–3188.
- (27) Lacroix, E.; Kortemme, T.; Paz, M.; Serrano, L. *Curr. Opin. Struct. Biol.* **1999**, *9*, 487–493.
- (28) Ho, B.; Dill, K. A. *PLoS Comput. Biol.* **2006**, *2*, 228–237.
- (29) Gunasekaran, K.; Ramakrishnan, C.; Balaram, P. *Protein Eng.* **1997**, *10*, 1131–1141.
- (30) Alvarado, R. M.; Blanco, F. J.; Niemann, H.; Serrano, L. *J. Mol. Biol.* **1997**, *273*, 898–912.
- (31) Chen, P.; Lin, C.; Lee, C.; Jan, H.; Chan, S. *Protein Sci.* **2001**, *10*, 1794–1800.
- (32) Wang, H.; Sung, S. *Biopolymers* **1999**, *50*, 763–776.
- (33) Alba, d. E.; Rico, M.; Jimenez, A. M. *Protein Sci.* **1999**, *8*, 2234.
- (34) Blanco, F. J.; Ramirez-Alvarado, M.; Serrano, L. *Curr. Opin. Struct. Biol.* **1998**, *8*, 107.
- (35) Du, D.; Zhu, Y.; Huang, C.; Gai, F. *Proc. Natl. Acad. Sci. U.S.A.* **2004**, *101*, 15915–15920.
- (36) Jones, S. R.; Maynard, A. J.; Searle, M. S. *J. Mol. Biol.* **1999**, *292*, 1051–1069.
- (37) Mahalakshmi, R.; Raghothama, S.; Balaram, P. *J. Am. Chem. Soc.* **2006**, *128*, 1125–1138.
- (38) Imamura, H.; Chen, J. Z. Y. *Proteins: Struct., Funct., Bioinf.* **2006**, *63*, 555.
- (39) Ramirez-Alvarado, M.; Blanco, F. J.; Serrano, L. *Nat. Struct. Biol.* **1996**, *3*, 604.
- (40) Ramirez-Alvarado, M.; Kortemme, T.; Blanco, F. J.; Serrano, L. *Bioorg. Med. Chem.* **1999**, *7*, 93.
- (41) Ma, B.; Nussinov, R. *J. Mol. Biol.* **2000**, *296*, 1091–1104.
- (42) Santiveri, C.; Rico, M.; Jimenez, A. *Protein Sci.* **2000**, *9*, 2151–2160.
- (43) Searle, M. S. *Biopolymers* **2004**, *76*, 185–195.
- (44) Hatfield, M. P. D.; Murphy, R. F.; Lovas, S. *J. Phys. Chem. B* **2010**, *114*, 3028–3037.
- (45) Bonvin, A. M. J. J.; van Gunsteren, W. *J. Mol. Biol.* **2000**, *296*, 255–268.
- (46) Chen, C.; Xiao, Y. *Phys. Biol.* **2006**, *3*, 161–171.
- (47) Bryant, Z.; Pande, V. J.; Rokhsar, D. S. *Biophys. J.* **2000**, *78*, 584–589.

- (48) Daidone, I.; Amadei, A.; Nola, A. *Proteins: Struct., Funct., Bioinf.* **2005**, *59*, 510–518.
- (49) Lee, J.; Shin, S. *Biophys. J.* **2001**, *81*, 2507–16.
- (50) Pande, V.; Rokhsar, D. *Proc. Natl. Acad. Sci. U.S.A.* **1999**, *96*, 9062–9067.
- (51) Santiveri, C. M.; Jimenez, M. A.; Rico, M.; Van Gunsteren, W. F.; Daura, X. *J. Pept. Sci.* **2004**, *10*, 546–565.
- (52) Wang, H.; Varady, J.; Ng, L.; Sung, S. *Proteins: Struct., Funct., Bioinf.* **1999**, *37*, 325–333.
- (53) Yoda, T.; Sugita, Y.; Okamoto, Y. *Proteins: Struct., Funct., Bioinf.* **2007**, *66*, 846–859.
- (54) Zagrovic, B.; Sorin, E. J.; Pande, V. *J. Mol. Biol.* **2001**, *313*, 151–169.
- (55) Nguyen, P.; Stock, G.; Mittag, E.; Hu, C.; Li, M. S. *Proteins: Struct., Funct., Bioinf.* **2005**, *61*, 795–808.
- (56) Wu, X.; Brooks, B. R. *Biophys. J.* **2004**, *86*, 1946–1958.
- (57) Knecht, V. *J. Phys. Chem. B* **2008**, *112*, 9476–9483.
- (58) Zhou, R. H.; Berne, B. J.; Germain, R. *Proc. Natl. Acad. Sci. U.S.A.* **2001**, *98*, 14931.
- (59) Nymeyer, H. *J. Phys. Chem. B* **2009**, *113*, 8288–8295.
- (60) Smith, A. W.; Lessing, J.; Ganim, Z.; Peng, C. S.; Tokmakoff, A.; Roy, S.; Jansen, T. L. C.; Knoester, J. *J. Phys. Chem. B* **2010**, *114*, 10913–10924.
- (61) Personal correspondence. See following papers from Tu's group for similar molecules: Leon, L.; Logrippo, P.; Tu, R. *Biophys. J.* **2010**, *99*, 2888. Leon, L.; Su, W.; Matsui, H.; Tu, R. *Soft Matter* **2011**, *7*, 10285–10290.
- (62) Hess, B.; Kutzner, C.; van der Spoel, D.; Lindahl, E. *J. Chem. Theory Comput.* **2008**, *4*, 435–447.
- (63) Berendsen, H. J. C.; Postma, J. P.; van Gunsteren, W. F.; Dinola, A.; Haak, J. R. *J. Chem. Phys.* **1984**, *81*, 3684–90.
- (64) Oostenbrink, C.; Villa, A.; Mark, A. E.; van Gunsteren, W. F. *J. Comput. Chem.* **2004**, *25*, 1656–76.
- (65) Berendsen, H. J. C.; Grigera, J. R.; Straatsma, T. P. *J. Phys. Chem.* **1987**, *91*, 6269.
- (66) Hess, B.; van der Vegt, N. F. A. *J. Phys. Chem. B* **2006**, *110*, 17616–17626.
- (67) Miyamoto, S.; Kollman, P. A. *J. Comput. Chem.* **1992**, *13*, 952–962.
- (68) Hess, B. *J. Chem. Theory Comput.* **2008**, *4*, 116–122.
- (69) Darden, T.; York, D.; Pedersen, L. *J. Chem. Phys.* **1993**, *98*, 10089–10092.
- (70) Yeh, I. C.; Berkowitz, M. L. *J. Chem. Phys.* **1999**, *111*, 3155–3162.
- (71) Kabsch, W.; Sander, C. *Biopolymers* **1983**, *22*, 2577.
- (72) Vriend, G. *J. Mol. Graphics* **1990**, *8*, 52–56.
- (73) Humphrey, W.; Dalke, A.; Schulten, K. *J. Mol. Graphics* **1996**, *14*, 33–38.
- (74) Hess, B. *J. Chem. Phys.* **2002**, *116*, 209.
- (75) Patey, G. N.; Valleau, J. P. *Chem. Phys. Lett.* **1973**, *21*, 297.
- (76) Torrie, G. M.; Valleau, J. P. *Chem. Phys. Lett.* **1974**, *28*, 578.
- (77) Kumar, S.; Rosenberg, J. M.; Bouzida, D.; Swendsen, R. H.; Kollman, P. A. *J. Comput. Chem.* **1992**, *13*, 1011–1021.
- (78) Hub, J. S.; Groot, B. L. *Biophys. J.* **2006**, *91*, 842–848.
- (79) Engin, O.; Villa, A.; Sayar, M.; Hess, B. *J. Phys. Chem. B* **2010**, *114*, 11093–11101.
- (80) Engin, O.; Sayar, M. Investigation of Structure of Amphipathic Peptides in Different Environments via Replica Exchange Molecular Dynamics Simulations. *From Computational Biophysics to Systems Biology (CBSB08), Proceedings of the NIC Workshop*, **2008**.